Supporting information

Highly aligned microgrid structure for wearable nanofibrous sensors with enhanced sensitivity and detection range

Mingxu Wang, [ab] Jiajia Wu, [ab] Li Dong, [ab], Jian Shi, [d] Qiang Gao, [e] Chunhong Zhu*[abc], Hideaki Morikawa*[abc]

[a]*Graduate School of Medicine, Science and Technology, Shinshu University, Tokida, Ueda, Nagano, 386-8567 Japan*

[b]*Institute for Fiber Engineering (IFES), Interdisciplinary Cluster for Cutting Edge Research (ICCER), Shinshu University, 3-15-1 Tokida, Ueda, Nagano 386-8567, Japan*

[c]*Faculty of Textile Science and Technology, Shinshu University, 3-15-1 Tokida, Ueda, Nagano 386-8567, Japan*

[d]*Faculty of Systems Science and Technology, Akita Prefectural University, 84-4 Aza Ebinokuchi, Tsuchiya, Yurihonjo, Akita, 015-0055, Japan*

[e]*School of Chemistry and Chemical Engineering, Yangzhou University, Yangzhou, 225002, China*

***Corresponding author**: Dr. Chunhong Zhu (zhu@shinshu-u.ac.jp), Dr. Hideaki Morikawa (morikaw@shinshu-u.ac.jp)*

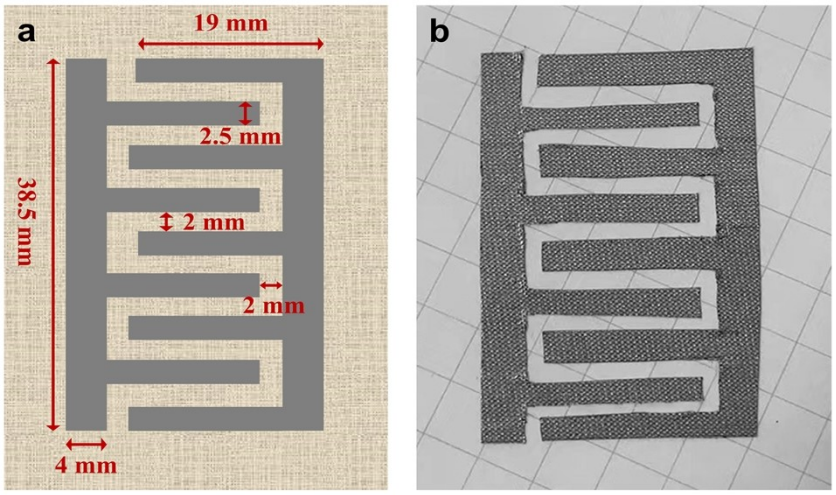

Fig. S1 (a) The design and parameters of the interdigitated electrodes. (b) Photograph of interdigitated electrodes.

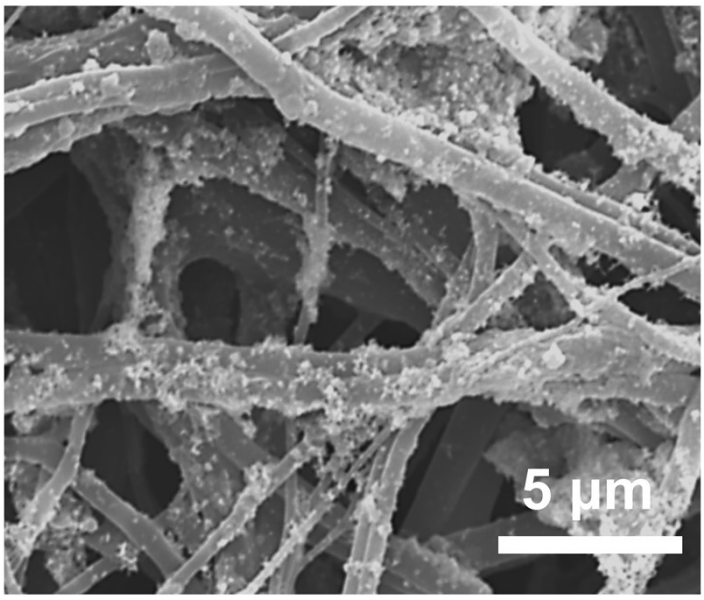

Fig. S2 SEM images of s-MXene embedded nanofiber membrane

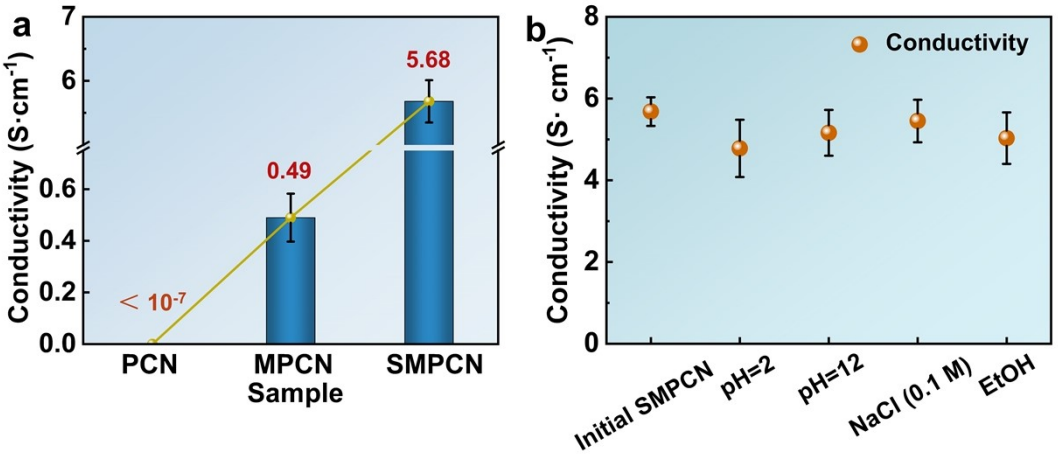

Fig. S3 (a) Conductivity of prepared nanofiber membrane. (b) Conductivity of the SMPCN nanofiber membrane after 6 hours in various harsh conditions.

For conductivity, samples were placed on the polytetrafluoroethylene (PTFE) plate and the two sections were fixed with silver paste. Until fully dried, the resistance is obtained by contacting the positive and negative probes of the digital multimeter with silver glue. The electroconductivity was calculated by the formula: $\sigma = L/(R \cdot S)$, where L, R and S denote the length, resistance and sectional area of test sample, respectively.

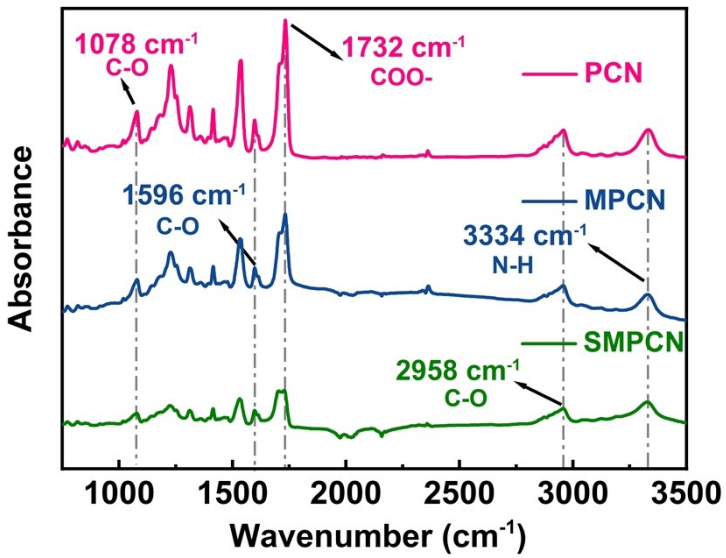

Fig. S4 FT-IR spectrogram of prepared nanofiber membrane

As shown in **Fig. S4**, for PCN membrane, characteristic bands at 1078 cm^{-1}, 1596 cm^{-1} and 1732 cm^{-1} correspond to the stretching vibration of C-O, plane bending vibration of N-H and the free hydrogen-bonded carbonyl groups in the urethane linkage (-H-N-COO-) in the spectrum of polyurethane (PU). Besides, obvious peaks of 2958 cm^{-1} and 3334 cm^{-1} belong to the stretching vibration of $-CH_3$ and overlap stretching vibration of N-H. The modification of CNTs, MXene and sliver do not change the position of the infrared peaks. However, clearly it can be observed that peak intensity of MPCN and SMPCN membrane decrease due to the presence of an external conductive layer.

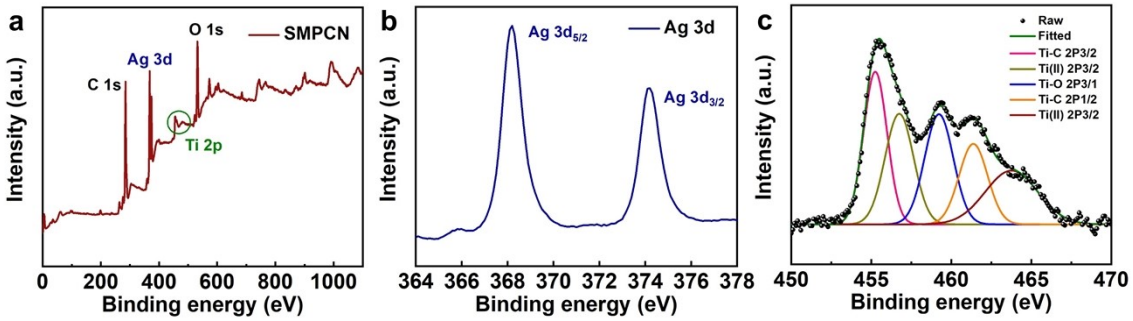

Fig. S5 XPS spectrogram of prepared nanofiber membrane

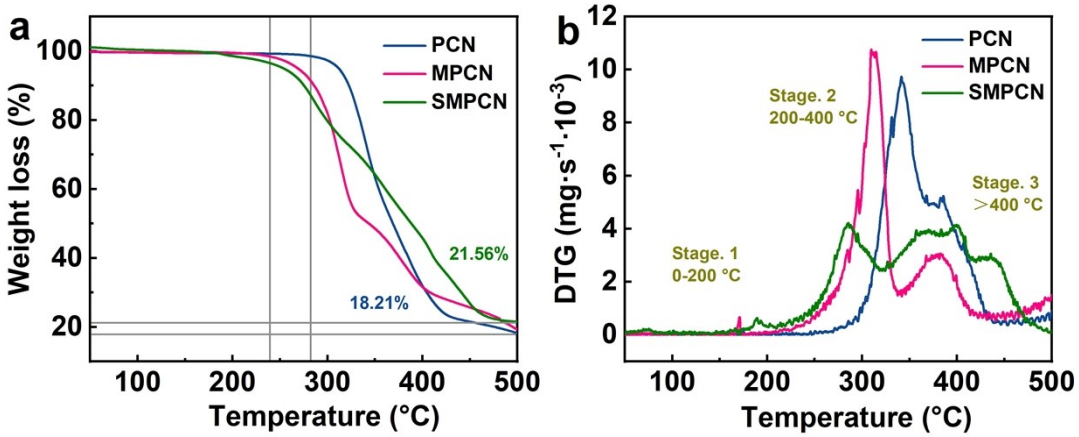

Fig. S6 TG and DTG curves of prepared nanofibers membrane

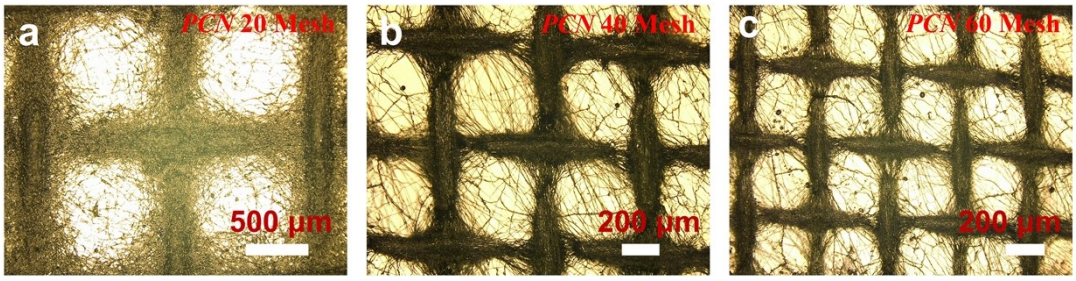

Fig. S7 SEM images of PCN membranes with different mesh

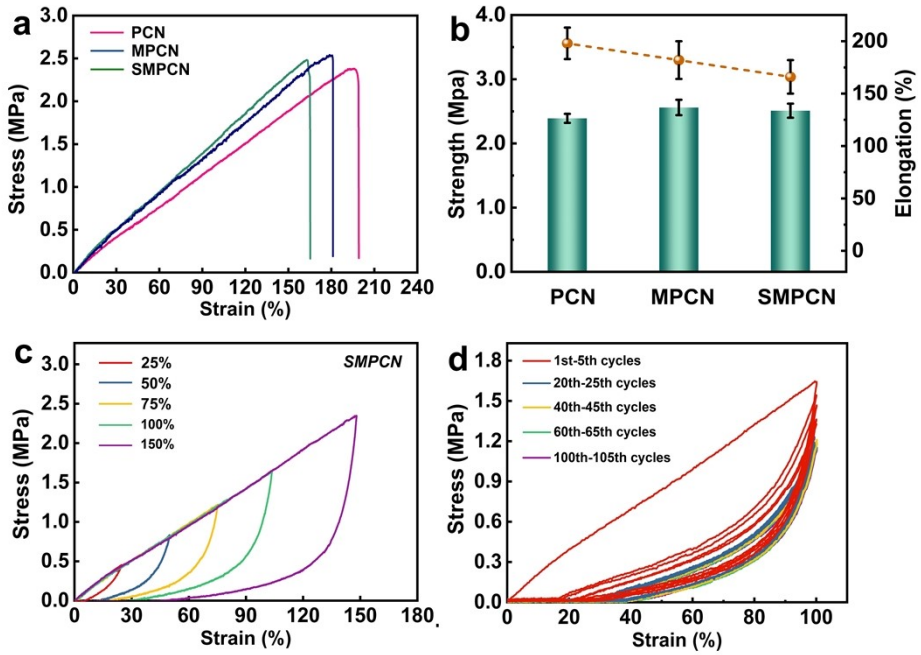

Fig. S8 Mechanical properties of prepared nanofibers. (a, b) Typical strain-stress curves and performance value of prepared nanofiber membrane. (c) The loading-unloading curves during different strains of SMPCN nanofibers membrane. (d) The tensile cycle test under 100% stretching for 100 times.

Fig. S8a shows typical strain-stress curves of prepared nanofibers membranes. Clearly, after the electrical activation process, the MPCN and SMPCN nanofiber membrane exhibit a reduced breaking elongation, approximately 20-40% compared to the initial sample (**Fig. S8b**). The breaking strength is basically constant. For another, compared with PU-based nanofiber membranes widely reported in other reference (~4 MPa and ~350%). Because of an extreme pursuit of thickness (~20 μm), microgrid skeletons bear most of the tensile stress. Thus, the mechanical properties of the SMPCN membrane are weak owing to the lack of sufficient entanglements between the single fiber. In addition, the cyclic tensile stress-strain curve of SMPCN sample is shown in the **Fig. S8c**. The stress is observed to increase slowly without a sudden increase of stress, when the tensile rate increase. Due to the non-oriented nanofibers distribution of the membrane, the elasticity is relatively poor, showing a dissipation of a larger amount of energy and hysteresis loop during the cyclic stretch-recovery process. However, the hysteresis remained stable for over 100 times after initial 20 cycles in the cyclic test (**Fig. S8d**).

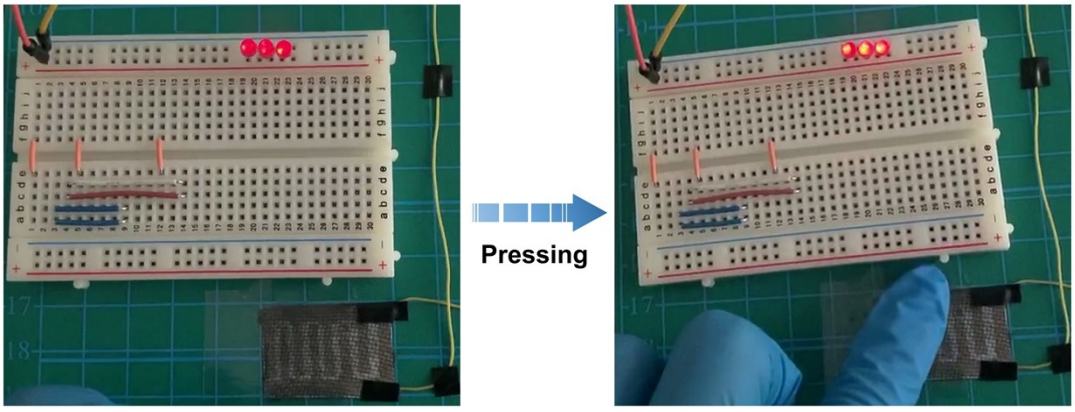

Fig. S9 Variation in the brightness of LED bulbs when pressure is applied

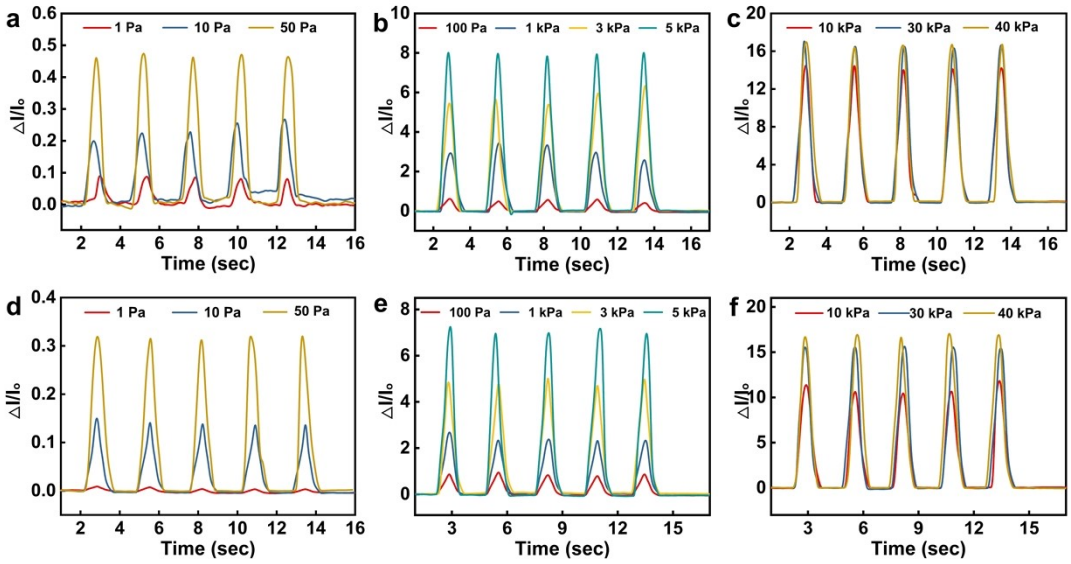

Fig. S10 Relative current response of the SMPCN pressure sensor (a-c: 20 mesh; d-f: 60 mesh) under cyclic loading/unloading with the pressure from 1Pa to 40 kPa.

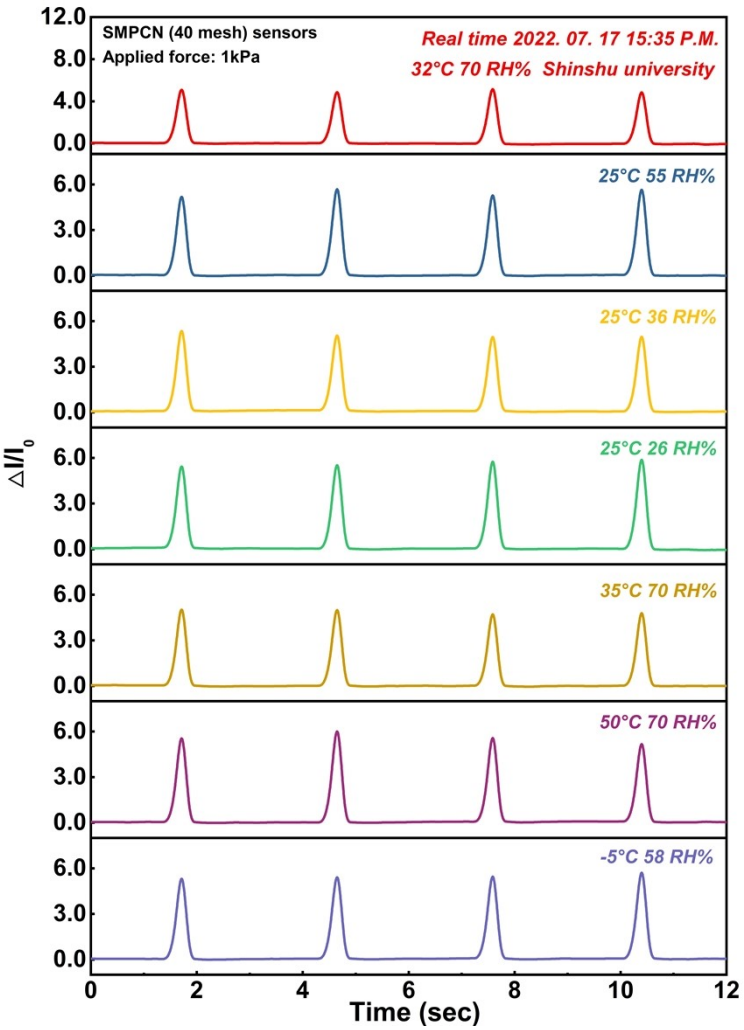

Fig. S11 Relative current response of the SMPCN pressure sensor (40 mesh) in different temperature and humidity.

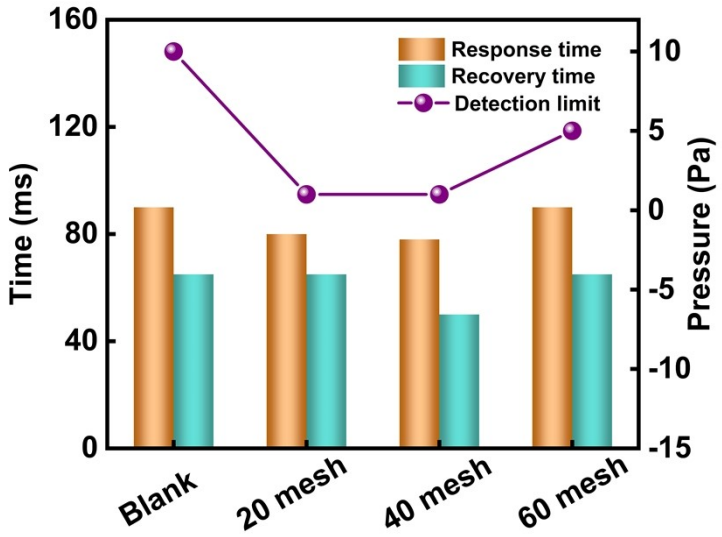

Fig. S12 Comparations of response/recovery time and detection limit of prepare SMPCN sensors.

Table. S1. Performance criteria comparison of microstructured or MXene-based tactile sensor

Ref.	Description	Methods	Mechanism	GF value (kPa^{-1})	Linear range (kPa)	Limit (Pa)
S1	Hierarchical micro-bulges	Laser process	Piezoresistive	0.90 11.06 4.5	0-0.6 0.6-10 10-30	—
S2	Nanofibrous sensors with HMs	In situ polymerization	Piezoresistive	20.60 0.89 0.15	0-1.0 1.0-8.0 8.0-20	~5.0
S3	Interlocked microarrays	Molding and coating	Piezoresistive	10.41 1.80	0-2.5 2.5-32	~1.0
S4	MXene-based aerogels	Directed freeze-casting and annealing	Piezoresistive	12.50	0-10	~1.0
S5	MXene-based Nanofibrous sensors	Template replication and spin coating	Piezoresistive	5.5	0-30	~2.0
S6	Aligned ridge micropatterns	Template replication and molding	Piezoresistive	10.0 3.3 0.33	0-0.4 0.4-1.0 1.0-7.0	~1.0
S7	Hierarchical protuberances	Template replication and CVD	Piezoresistive	19.8 0.27	0-0.3 0.3-6.0	~0.6
S8	Hierarchical micro-crumples	Template replication and self-stress relaxation	Piezoelectric	2.35 0.14	0-0.9 0.9-25	—
S9	MXene-based tissue paper sensors	Soaking	Piezoresistive	0.55 3.81 2.12	0-1.0 1.0-10 13-30	~10.2
S10	Nanofibrous sensors with HMs	Spin coating	Piezocapacitive	1.21 0.15	0-3.0 3.0-27	~0.9
S11	Microarrays	Soaking and interface diffusion	Piezoresistive	2.18 1.8 0.5	0-0.025 0.025-2.0 2.0-6.0	~2.5
S12	Hierarchical corrugated structure	Carbonization	Piezoresistive	5.67 2.52 0.87 0.32	0-0.42 0.43-2.53 2.53-9.06 9.06-20	~0.9

S13	Hierarchical pillar arrays	Template replication	Piezocapacitive	14.5 0.56	0-10 10-50	—
This work	**Hierarchical micro-grids**	**Template replication**	**Piezoresistive**	**15.3** **1.68** **0.15**	**0-0.1** **0.1-10** **10-40**	**~1.0**

References for supporting information

S1 C. Zhang, R. Chen, C. Xiao, H. Zhao, Y. Wang, D. Geng, S. Chen, T. Luo and W. Zhou, *Adv Materials Inter*, 2022, **9**, 2101596.

S2 K. Qi, J. He, H. Wang, Y. Zhou, X. You, N. Nan, W. Shao, L. Wang, B. Ding and S. Cui, *ACS Appl. Mater. Interfaces*, 2017, **9**, 42951–42960.

S3 T.-Y. Hwang, Y. Choi, Y. Song, N. S. A. Eom, S. Kim, H.-B. Cho, N. V. Myung and Y.-H. Choa, *J. Mater. Chem. C*, 2018, **6**, 972–979.

S4 Z. Chen, Y. Hu, H. Zhuo, L. Liu, S. Jing, L. Zhong, X. Peng and R. Sun, *Chem. Mater.*, 2019, **31**, 3301–3312.

S5 S. Sharma, A. Chhetry, S. Zhang, H. Yoon, C. Park, H. Kim, Md. Sharifuzzaman, X. Hui and J. Y. Park, *ACS Nano*, 2021, **15**, 4380–4393.

S6 P. Nie, R. Wang, X. Xu, Y. Cheng, X. Wang, L. Shi and J. Sun, *ACS Appl. Mater. Interfaces*, 2017, **9**, 14911–14919.

S7 M. Jian, K. Xia, Q. Wang, Z. Yin, H. Wang, C. Wang, H. Xie, M. Zhang and Y. Zhang, *Adv. Funct. Mater.*, 2017, **27**, 1606066.

S8 Y. Cao, Y. Guo, Z. Chen, W. Yang, K. Li, X. He and J. Li, *Nano Energy*, 2022, 92, 106689.

S9 Y. Guo, M. Zhong, Z. Fang, P. Wan and G. Yu, *Nano Lett.*, 2019, **19**, 1143–1150.

S10 S. Zhao, W. Ran, D. Wang, R. Yin, Y. Yan, K. Jiang, Z. Lou and G. Shen, *ACS Appl. Mater. Interfaces*, 2020, **12**, 32023–32030.

S11 D. Yao, L. Wu, S. A, M. Zhang, H. Fang, D. Li, Y. Sun, X. Gao and C. Lu, *Chem Eng J,* 2022, **431**, 134038.

S12 S. Chen, Y. Song and F. Xu, *ACS Appl. Mater. Interfaces*, 2018, **10**, 34646–34654.

S13 M. L. Jin, S. Park, Y. Lee, J. H. Lee, J. Chung, J. S. Kim, J.-S. Kim, S. Y. Kim, E. Jee, D. W. Kim, J. W. Chung, S. G. Lee, D. Choi, H.-T. Jung and D. H. Kim, *Adv. Mater.*, 2017, **29**, 1605973.